JACS
JOURNAL OF THE AMERICAN CHEMICAL SOCIETY
Communication
pubs.acs.org/JACS

Solution-Processed Organic Solar Cells Based on Dialkylthiol-Substituted Benzodithiophene Unit with Efficiency near 10%

Bin Kan,[†] Qian Zhang,[†] Miaomiao Li, Xiangjian Wan, Wang Ni, Guankui Long, Yunchuang Wang, Xuan Yang, Huanran Feng, and Yongsheng Chen*

Key Laboratory of Functional Polymer Materials and the Center for Nanoscale Science and Technology, Institute of Polymer Chemistry, College of Chemistry, Collaborative Innovation Center of Chemical Science and Engineering (Tianjin), Nankai University, Tianjin 300071, China

Supporting Information

ABSTRACT: A small molecule named DR3TSBDT with dialkylthiol-substituted benzo[1,2-*b*:4,5-*b*′]dithiophene (BDT) as the central unit was designed and synthesized for solution-processed bulk-heterojunction solar cells. A notable power conversion efficiency of 9.95% (certified 9.938%) has been achieved under AM 1.5G irradiation (100 mW cm^{-2}), with an average PCE of 9.60% based on 50 devices.

Organic photovoltaics (OPVs) have been thought of as a promising next-generation green technology with advantages such as solution processability, lightweight, low cost, and flexibility.[1,2] With the rapid progress over recent years, power conversion efficiencies (PCEs) over 9% have been achieved for polymer based OPVs (P-OPVs) with bulk-heterojunction (BHJ) architecture.[3−6] Compared to the widely investigated P-OPVs,[6−10] solution processed small molecule based OPVs (SM-OPVs) have made great strides[11−14] and a PCE over 8% has been achieved in recent years for a single-junction solar cell[12,15,16] and a PCE of 10.1% for tandem cell devices.[17] In view of the advantages of small molecules including versatile chemical structures, and thus easier energy level control, mobility tuning, and less batch-to-batch variation,[18,19] it is believed that higher performance could be obtained for SM-OPVs.

Currently, photoactive material innovation, especially for donors, and device optimization are the two key points to obtain high performance for both polymer and small molecule based OPVs.[6] For the design of donor materials, several issues should be considered altogether and with a delicate balance: good solubility, wide and efficient absorption, suitable energy levels, and high mobility.[20] Among the device optimization conditions, morphology control to achieve a nanoscale interpenetrating network of donor and acceptor phases with proper domain sizes on the order of tens of nanometers is the necessary and determining factor.[21−23]

Recently, we have reported a series of benzo[1,2-*b*:4,5-*b*′]dithiophene (BDT) based small molecules. Through delicate molecule design mainly at the BDT unit and device optimization, a PCE over 8% was obtained.[24] These encouraging results together with the high performances of BDT based polymer OPV devices indicate that BDT is an excellent building block for SM-OPVs. Thus, designing new molecules by incorporating and/or modifying a BDT unit might result in further advancements for SM-OPVs. The sulfur atom possesses weaker electron-donating ability than that of an oxygen atom. An alkylthio side chain has been employed in organic semiconductors, which exhibit some unique optoelectronic properties and more ordered molecule packing.[5,25−27] Furthermore, it has been demonstrated that a dialkylthiol-substituted BDT homopolymer exhibits better photovoltaic performance than its dialkyloxy-substituted counterparts.[28,29] Herein, based on our previous results for DR3TBDT,[30] we designed and synthesized a new small molecule, DR3TSBDT, with dialkylthiol-substituted BDT as the central building block for solution processed SM-OPVs. As shown in Figure 1a, DR3TSBDT demonstrates a similar chemical structure compared with DR3TBDT except for the replacement of oxygen with a sulfur atom in the BDT side chains. Remarkably, such a small change has resulted in an optimized PCE of 9.95% (certified 9.938%) achieved for the DR3TSBDT/$PC_{71}BM$

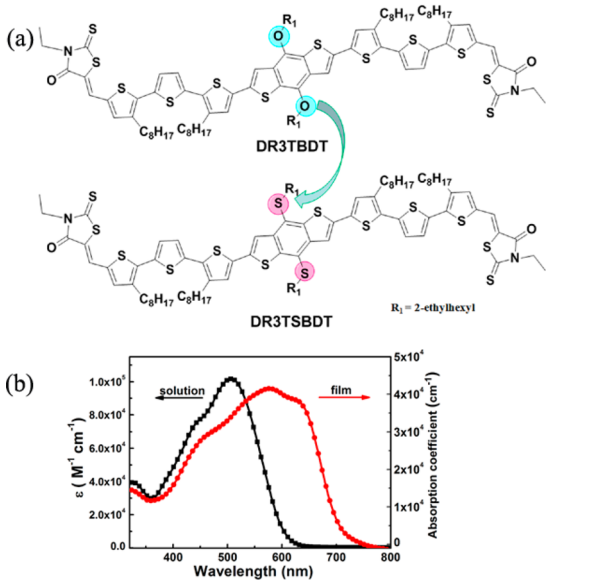

Figure 1. (a) Chemical structures of DR3TBDT and DR3TSBDT; (b) UV−vis absorption spectra of DR3TSBDT solution and film.

Received: September 25, 2014
Published: October 22, 2014

   dx.doi.org/10.1021/ja509703k | J. Am. Chem. Soc. 2014, 136, 15529−15532

based OPV devices, which is so far the highest PCE for single-junction OPVs with the average PCE of 50 devices at 9.60%.

The detailed synthetic procedures and the characterization data for DR3TSBDT are presented in the Supporting Information (SI). The molecule exhibits good solubility in common organic solvents, such as chloroform, chlorobenzene, and etc., and good film-forming ability. Thermogravimetric analysis (TGA) suggests that DR3TSBDT has excellent thermal stability up to 370 °C under a N_2 atmosphere (Figure S1).

The UV−vis absorption spectra of DR3TSBDT in diluted $CHCl_3$ solution and in solid film are shown in Figure 1b. The absorption of DR3TSBDT solution shows a peak at 508 nm and a maximum absorption coefficient of 1.01×10^5 M^{-1} cm^{-1}. In solid film, the spectrum was broadened and red-shifted with a maximum absorption coefficient of 4.2×10^4 cm^{-1} at 586 nm. Besides, an obvious vibronic shoulder peak at 633 nm was observed, which indicates effective $\pi-\pi$ stacking between molecule backbones. The optical band gap estimated from the onset of the film absorption is 1.74 eV. The DR3TSBDT exhibits similar optical properties to those of DR3TBDT but with a higher maximum absorption coefficient both in solution (Figure S2 and Table S1). The cyclic voltammetry was used to investigate the energy levels (Figure S3). The potentials were internally calibrated using the ferrocene/ferrocenium of the (Fc/Fc^+) redox couple (4.8 eV below the vacuum level). The energy levels of the HOMO calculated from the onset oxidation potential is -5.07 ± 0.02 eV, which is slightly lower than that of DR3TBDT. The electrochemical band gap of DR3TSBDT is estimated to be about 1.77 eV, which is in agreement with its optical band gap. These results are also consistent with our density functional theory (DFT) calculation results using the B3LYP/6-31G(d) model (Table S2). The above data suggest that DR3TSBDT with the dialkylthio-substituted BDT unit would be a better donor for OPVs.

Solution-processed BHJ devices were fabricated using DR3TSBDT as the electron donor with a conventional device structure of ITO/PEDOT:PSS/DR3TSBDT:$PC_{71}BM$/ETL-1/Al. ETL-1 is a methanol-soluble fullerene-surfactant developed by Alex K.-Y as an efficient interfacial layer for cathodes,[31] and its structure is shown as Figure S4. The $J-V$ curves of the devices with different post-treatments were presented in Figure 2, and the corresponding photovoltaic parameters are summarized in Table 1. With a series of testing (SI), an optimal donor/acceptor weight ratio was obtained as 1:0.8, and the device without any treatment shows a moderate PCE of 6.62% with a V_{oc} of 0.96 V, a short-circuit current (J_{sc}) of 12.32 mA cm^{-2}, and a fill factor (FF) of 0.56. After thermal annealing (TA) at 100 °C for 10 min, the PCE increased to 7.99%, with a V_{oc} of 0.96 V, a J_{sc} of 13.41 mA cm^{-2}, and an FF of 0.62. As an effective approach, solvent vapor annealing (SVA) has been used in polymer based OSCs devices to fine-tune the morphology of the active layer.[32] Herein, the approach was employed in the device optimization in combination with TA. The active layer was exposed to chloroform vapor for 60 s after TA. Surprisingly, the PCE sharply improved to 9.95% (certified at 9.938%), with a V_{oc} of 0.92 V, a J_{sc} of 14.61 mA cm^{-2}, and an outstanding FF of 0.74. It is worth noting that, during preparation of this paper, Bäuerle reported that solvent vapor annealing also worked for their small molecule based devices.[33] This striking result was attributed to the significant improvement of J_{sc} and FF, which was originated from the enhanced absorption, preferable morphology, and higher and more balanced charge motilities as discussed below.

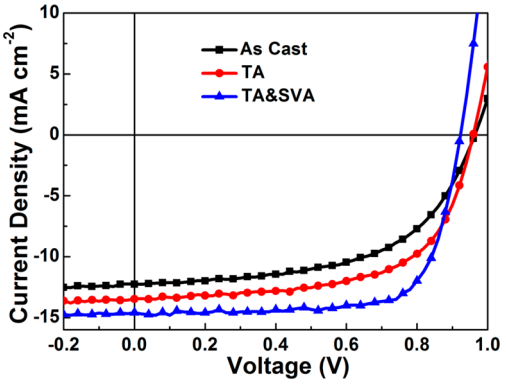

Figure 2. $J-V$ curves of devices without treatment (black), with TA treatment (red), and with TA and SVA treatment (blue).

In order to investigate the effect of TA and SVA on the device performance, UV−vis absorption spectra of blend films and the external quantum efficiency (EQE) were measured. As shown in Figure 3a, in comparison with the spectra of as-cast blend film, the spectra of the film with TA shows a red shift of 20 nm and exhibits an obvious shoulder peak at 636 nm, which is related to the enhanced $\pi-\pi$ stacking. For films with further SVA treatment, the absorption intensity overall increased, thus resulting in improved J_{sc}. As we used the same blend film for different treatments, the changes in absorption spectra are believed not to be due to the variation of film thickness. Besides, as illustrated from the EQE curves, uniform increases of the spectral response across the wavelength range of 300−800 nm are clearly observed for devices with TA treatment. Especially, for the device with dual TA and SVA treatment, the EQE was significantly improved again with a maximum value of 78% and over 75% across the range of 410−600 nm, which indicates that the photoelectron conversion process is highly efficient. These results are consistent with the trend of the above UV−vis absorption results. The calculated J_{sc} obtained by integration of the EQE curves are 11.78, 12.92, and 14.10 mA cm^{-2}, respectively, for the three different treatments, which show a 3−5% mismatch compared with the J_{sc} value obtained from the $J-V$ curves.

The morphology of the active layer was investigated by atomic force microscopy (AFM) and transmission electron microscopy (TEM). From AFM measurement (Figure S5), the root-mean-square (RMS) roughness is 0.62 nm for blend films without any treatment. After TA and further SVA treatment, it increases to 0.90 and 0.91 nm, respectively, which reveals that the films are smooth with high quality. Figure 4 shows the TEM images of the blend films. Compared with the as-cast film, better phase separation could be found after the TA process. With further SVA treatment, obvious nanoscale phase separation with an ∼15 nm domain size and a bicontinuous interpenetrating network can be clearly observed, which contributes to high exciton dissociation and charge transport efficiency.[34] Therefore, significantly improved J_{sc} and FF were achieved. The morphology of the pure and blend films with the above two annealing steps were further investigated by two-dimensional (2D) grazing-incidence wide-angle X-ray scattering (GIWAXS). As can be seen from Figure S6, the reflection intensity of both (h00) and (010) was strengthened for both pure and blend films with TA and SVA treatment, which indicates that a more ordered structure was formed with these

dx.doi.org/10.1021/ja509703k | J. Am. Chem. Soc. 2014, 136, 15529−15532

Table 1. Average Device Performance Parameters for BHJ Solar Cells Based on DR3TSBDT[a]

treatment	V_{oc} (V)	J_{sc} (mA cm^{-2})	*FF*	PCE (%)
none	0.96 ± 0.01	11.87 ± 0.44	0.56 ± 0.01	6.38 ± 0.24(6.62)
TA	0.96 ± 0.01	13.00 ± 0.40	0.61 ± 0.02	7.61 ± 0.38(7.99)
TA + SVA	0.91 ± 0.01	14.45 ± 0.18	0.73 ± 0.01	9.60 ± 0.35(9.95)

[a]The average values are obtained from over 50 devices. The best PCEs are provided in parentheses.

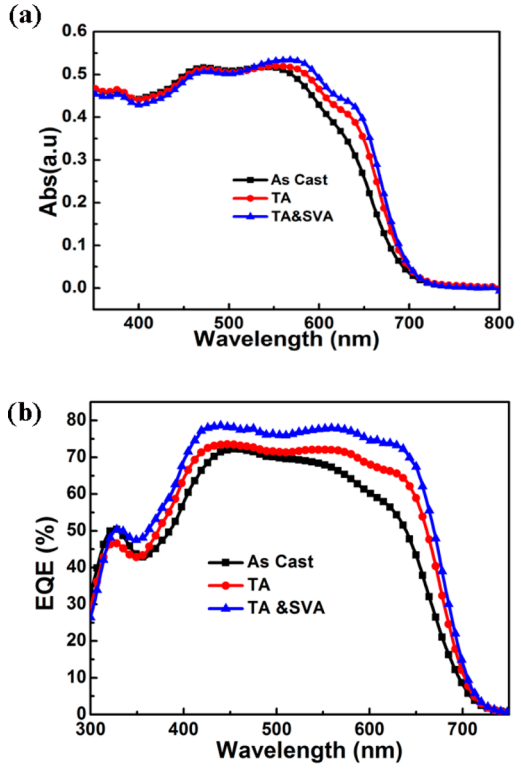

Figure 3. (a) UV−vis absorption spectra of DR3TSBDT:$PC_{71}BM$ blend with different treatments; (b) EQE curves of DR3TSBDT-based devices with different treatments.

treatments, and this should promote efficient charge transport and lead to a high *FF*.[35]

The mobilities of the blend films were measured by the space charge limited current (SCLC) method (Figure S7). For devices without any treatment, the hole and electron mobility were 1.33 × 10^{-4} and 1.59 × 10^{-4} cm^2 V^{-1} s^{-1}, respectively. After TA, the hole and electron mobility increased to 3.02 × 10^{-4} and 1.86 × 10^{-4} cm^2 V^{-1} s^{-1}, respectively. Additionally, the device with further SVA exhibits a higher and much more balanced hole and electron mobility of 6.13 × 10^{-4} and 4.84 × 10^{-4} cm^2 V^{-1} s^{-1}, respectively, which is favorable for a higher *FF*. To further probe the charge recombination in the optimal device, the light intensity dependence of *J*−*V* characteristics was measured. Figure S8 shows a linear relation of photocurrent to light intensity in a double logarithmic scale at both low effective voltage (0.3 V) and high effective voltage (1.9 V), the slopes of which are 0.95 and 1, respectively. This suggests that bimolecular recombination loss is rather minor, supporting a high *FF*.[36]

In summary, a new small molecule donor material DR3TSBDT containing a central dialkylthio-substituted BDT unit was designed and synthesized. With TA and SVA treatment, a notable PCE of 9.95% was achieved with an average PCE at 9.60%, which was attributed to the enhancement of the absorption of blend films and a preferable morphology. This is so far the highest PCE reported for single-junction OPVs. For the diversity of molecule design, together with the device optimization, further improvement would be highly expected. With the great boost in PCEs, other factors, such as manufacturing cost, lifetime, form factor, weight, scalability, and sustainable manufacturing, should receive increasing attention for the application of OPVs.

■ ASSOCIATED CONTENT

Supporting Information

Detailed synthetic procedures and characterization data for the new compounds; OPV device fabrication process and data; and additional experimental results. This material is available free of charge via the Internet at http://pubs.acs.org.

■ AUTHOR INFORMATION

Corresponding Author

yschen99@nankai.edu.cn

Author Contributions

†B.K. and Q.Z. contributed equally.

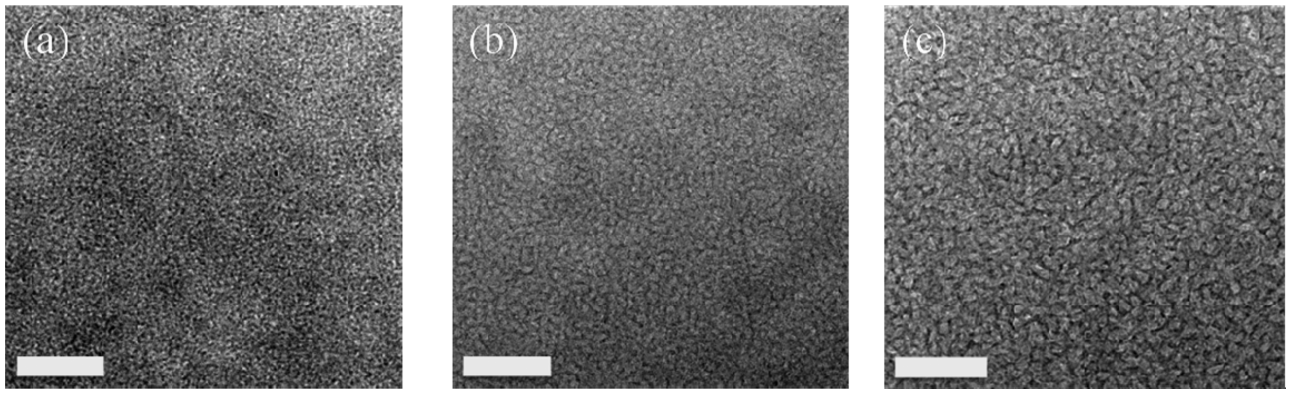

Figure 4. TEM images of active layer based on DR3TSBDT:$PC_{71}BM$ (a) as cast; (b) with TA; and (c) with TA and SVA. The scale bar is 200 nm.

dx.doi.org/10.1021/ja509703k | J. Am. Chem. Soc. 2014, 136, 15529−15532

Notes

The authors declare no competing financial interest.

■ ACKNOWLEDGMENTS

The authors gratefully acknowledge financial support from the MOST (Grants 2012CB933401 and 2014CB643502), NSFC (Grants 50933003, 51273093, and 21004043), NSF of Tianjin City (Grant 10ZCGHHZ00600), and PCSIRT (IRT1257) and thank beamline BL14B1 (Shanghai Synchrotron Radiation Facility) for providing beam time.

■ REFERENCES

(1) Peumans, P.; Yakimov, A.; Forrest, S. R. *J. Appl. Phys.* **2003**, *93*, 3693.
(2) Service, R. F. *Science* **2011**, *332*, 293.
(3) He, Z.; Su, S.; Xu, M.; Wu, H.; Cao, Y. *Nat. Photonics* **2012**, *6*, 591.
(4) Liao, S.; Huo, J.; Cheng, Y.; Chen, S. *Adv. Mater.* **2013**, *25*, 4766.
(5) Ye, L.; Zhang, S.; Zhao, W.; Yao, H.; Hou, J. *Chem. Mater.* **2014**, *26*, 3306.
(6) Dou, L.; You, J.; Hong, Z.; Xu, Z.; Li, G.; Street, R. A.; Yang, Y. *Adv. Mater.* **2013**, *25*, 6642.
(7) Liang, Y.; Yu, L. *Acc. Chem. Res.* **2010**, *43*, 1227.
(8) Zhou, H.; Yang, L.; You, W. *Macromolecules* **2012**, *45*, 607.
(9) Li, Y. *Acc. Chem. Res.* **2012**, *45*, 723.
(10) Guo, X.; Zhou, N.; Lou, S. J.; Smith, J.; Tice, D.; Hennek, J.; Ponce Ortiz, R.; Lopez Navarrete, J.; Li, S.; Strzalka, J.; Chen, L.; Chang, R.; Facchetti, A.; Marks, T. J. *Nat. Photonics* **2013**, *7*, 825.
(11) Mishra, A.; Bäuerle, P. *Angew. Chem., Int. Ed.* **2012**, *51*, 2020.
(12) Lin, Y.; Li, Y.; Zhan, X. *Chem. Soc. Rev.* **2012**, *41*, 4245.
(13) Sun, Y.; Welch, G.; Leong, W.; Takacs, C.; Bazan, G. C.; Heeger, A. J. *Nat. Mater.* **2012**, *11*, 44.
(14) Coughlin, J. E.; Henson, Z. B.; Welch, G. C.; Bazan, G. C. *Acc. Chem. Res.* **2014**, *47*, 257.
(15) Kyaw, A. K. K.; Wang, D. H.; Wynands, D.; Zhang, J.; Nguyen, T. Q.; Bazan, G. C.; Heeger, A. J. *Nano Lett.* **2013**, *13*, 3796.
(16) Zhou, J.; Zuo, Y.; Wan, X.; Long, G.; Zhang, Q.; Ni, W.; Liu, Y.; Li, Z.; He, G.; Li, C.; Kan, B.; Li, M.; Chen, Y. *J. Am. Chem. Soc.* **2013**, *135*, 8484.
(17) Liu, Y.; Chen, C.; Hong, Z.; Gao, J.; Yang, Y.; Zhou, H.; Dou, L.; Li, G.; Yang, Y. *Sci. Rep.* **2013**, *3*, 3356.
(18) Walker, B.; Kim, C.; Nguyen, T. Q. *Chem. Mater.* **2011**, *23*, 470.
(19) Roncali, J.; Leriche, P.; Blanchard, P. *Adv. Mater.* **2014**, *26*, 3821.
(20) Beaujuge, P. M.; Fréchet, J. M. J. *J. Am. Chem. Soc.* **2011**, *133*, 20009.
(21) Brabec, C. J.; Heeney, M.; McCulloch, I.; Nelson. *J. Chem. Soc. Rev.* **2011**, *40*, 1185.
(22) Dang, M. T.; Hirsch, L.; Wantz, G.; Wuest, J. D. *Chem. Rev.* **2013**, *113*, 3734.
(23) Huang, Y.; Kramer, E. J.; Heeger, A. J.; Bazan, G. C. *Chem. Rev.* **2014**, *114*, 7006.
(24) Chen, Y.; Wan, X.; Long, G. *Acc. Chem. Res.* **2013**, *46*, 2645.
(25) Huo, L.; Yi, Z.; Li, Y. *Macromol. Rapid Commun.* **2009**, *30*, 925.
(26) Li, K.; Li, Z.; Feng, K.; Xu, X.; Wang, L.; Peng, Q. *J. Am. Chem. Soc.* **2013**, *135*, 13549.
(27) Cui, C.; Wong, W. Y.; Li, Y. *Energy Environ. Sci.* **2014**, *7*, 2276.
(28) Lee, D.; Stone, S. W.; Ferraris, J. P. *Chem. Commun.* **2011**, *47*, 10987.
(29) Lee, D.; Hubijar, E.; Kalaw, G. J. D.; Ferraris, J. P. *Chem. Mater.* **2012**, *24*, 2534.
(30) Zhou, J.; Wan, X.; Liu, Y.; Zuo, Y.; Li, Z.; He, G.; Long, G.; Ni, W.; Li, C.; Su, X.; Chen, Y. *J. Am. Chem. Soc.* **2012**, *134*, 16345.
(31) Li, C. Z.; Chueh, C. C.; Yip, H. L.; O'Malley, K. M.; Chen, W. C.; Jen, A. K. Y. *J. Mater. Chem.* **2012**, *22*, 8574.
(32) Miller, S.; Fanchini, G.; Lin, Y. Y.; Li, C.; Chen, C. W.; Su, W. F.; Chhowalla, M. *J. Mater. Chem.* **2008**, *18*, 306.
(33) Wessendorf, C. D.; Schulz, G. L.; Mishra, A.; Kar, P.; Ata, I.; Weidelener, M.; Urdanpilleta, M.; Hanisch, J.; Mena-Osteritz, E.; Lindén, M.; Ahlswede, E.; Bäuerle, P. *Adv. Energy Mater.* **2014**, *4*, 1400266.
(34) Proctor, C. M.; Kuik, M.; Nguyen, T. Q. *Prog. Polym. Sci.* **2013**, *38*, 1941.
(35) Muller-Buschbaum, P. *Adv. Mater.*, DOI: 10.1002/adma.201304187.
(36) Lenes, M.; Morana, M.; Brabec, C. J.; Blom, P. W. M. *Adv. Funct. Mater.* **2009**, *19*, 1106.